JOURNAL OF MATERIALS SCIENCE 32 (1997) 6435–6445

The processing and characterization of sintered metal-reinforced aluminium matrix composites

R. P. BARON, J. A. WERT, D. A. GERARD[1], F. E. WAWNER
The Department of Materials Science and Engineering, University of Virginia, Charlottesville, VA 22903 and [1]Manager, Advanced Materials of Process Development, General Motors Powertrain Group, Saginaw MI 48605

The current investigation involves the fabrication and characterization of an aluminium metal matrix composite reinforced with sintered metal preforms. Two types of metallic preforms were used (steel and stainless steel) and a variety of squeeze casting conditions were investigated using systematic design-of-experiments techniques to determine the effect of casting conditions on the composite microstructure and mechanical properties. It was observed that a detrimental reaction phase containing iron, aluminium and silicon formed around the metallic preform particles, with a lower volume fraction of reaction phase forming at the lower melt casting temperature. This reaction phase appears to promote premature fracture by facilitating crack initiation and propagation. The stainless steel-reinforced composites had a smaller volume fraction of reaction phase and exhibited superior properties compared to the steel-reinforced composites.

1. Introduction

Much research has focused on the fabrication and properties of aluminium metal matrix composites (MMC) reinforced with ceramic preforms [1–4]. Metallic materials are also viable reinforcements, but several disadvantages inhibit their widespread utilization. First, in general, ceramic materials offer greater potential increases in strength and modulus when they are used as the reinforcing phase, compared to metallic reinforcements. Second, ceramic reinforcements are commonly less dense than metallic reinforcements, thereby producing lighter composites. Finally, metallic reinforcements can react with the metallic matrix, causing a degradation of the resulting composite properties. However, metallic materials may also provide benefits not offered by ceramic materials. For example, metallic reinforcements may not lower the ductility or toughness of the matrix phase as dramatically as ceramic reinforcements. Also, metallic reinforcements may provide a cost advantage compared to their ceramic counterparts. To explore these possibilities, several investigators have studied metallic reinforcements in an aluminium matrix [5–9].

Metal/metal composites can be fabricated by solid-state consolidation or by a liquid infiltration process. For example, Cratchley [5] and, more recently, Bhagat [6, 7] fabricated aluminium matrix composites reinforced with stainless steel wires by powder metallurgy (PM) techniques. Both authors produced practical composites with volume fractions of reinforcing phase as high as 0.4. The mechanical properties of the PM composites were substantially higher than the unreinforced aluminium metal, provided that the reaction between aluminium and stainless steel fibres was minimized. This required careful control of the consolidation time, temperature, and pressure.

Bhagat [8] has also used the squeeze casting technique to produce an aluminium matrix composite reinforced with stainless steel wires. By inducing intimate contact between the infiltrating metal and the die and reinforcement phase, squeeze, or pressure, casting facilitates rapid solidification and a reduction in the fibre-to-liquid metal contact time. As a result, the amount of reaction phase that forms during fabrication is decreased. The high pressures employed in squeeze casting also promote infiltration of the metal preform, thereby decreasing the final porosity within the composite. Thus, pressure casting can offer several advantages over the pressing and sintering techniques employed in powder metallurgy.

The formation of a reaction phase between aluminium and stainless steel fibres during composite fabrication via pressure casting was studied closely by Colin *et al.* [9]. A reduction in reaction-phase thickness surrounding the stainless steel fibres was observed in regions of short contact time between the liquid metal and stainless steel reinforcements, namely areas that were in contact with the die wall or that were the last to be infiltrated. Also, as the volume fraction of reinforcement increased, the amount of reaction phase decreased due to the increased cooling rate provided by the larger volume fraction of metallic reinforcement. In each of the investigations summarized here, the reaction phase was identified to be an Fe–Al intermetallic phase, but the exact composition and crystal structure were not determined.

Because the formation of a reaction phase is intimately connected to the infiltration of the liquid metal

0022–2461

into the preform, knowledge of the penetration kinetics is essential for successful fabrication of cast metal/metal composites. Mortensen and co-workers [10–14] have extensively studied the pressure casting process for metal matrix composites. The research has concentrated on analyses of fluid flow and heat transfer during the infiltration of fibrous ceramic preforms by pure and alloyed liquid aluminium. The relative density of the ceramic preforms varied between 0.20 and 0.26. In their study, no significant reaction occurred between the pure aluminium and Al_2O_3 fibres during high-temperature fabrication; but solidification did occur around the ceramic fibres, which inhibited subsequent liquid metal penetration by constricting or blocking channels through which the liquid metal was flowing. The volume fraction and initial temperature of the preform had the greatest effect on the infiltration kinetics of the pressure casting process, with the metal superheat and infiltration pressure having smaller effects. It was observed that an increase in the fibre volume fraction or a decrease in the preform temperature reduced the extent of penetration of the infiltration metal into the ceramic preform. Also, due to the high pressures involved, some of the ceramic preforms deformed during fabrication.

The objective of the present work was to describe the effects of the reinforcing phase composition and pressure casting parameters on the structure and properties of a metallic-reinforced aluminium composite. However, unlike previous investigations, metallic reinforcements in the form of low-density powder metallurgy preforms were used to reinforce the squeeze cast aluminium MMCs, instead of fibres. To provide the necessary strength and handability, the relative density of the PM preforms was approximately 0.6–0.7, which produced a much larger volume fraction of reinforcing phase than previously studied. Also, instead of using pure aluminium to infiltrate the PM preforms, a common aluminium casting alloy was used as the matrix phase.

2. Experimental procedure

2.1. Materials

In the present investigation, powder metallurgy steel preforms were used as the reinforcing phase. The preforms were fabricated by pressing and sintering steels of various compositions to produce flat, cylindrical porous preforms approximately 10.4 cm diameter and 1.5 cm tall. Anchor 1000™ iron powder (− 80 mesh) was used to produce steel preforms. Graphite powder was blended with the iron powder as a lubricant and pressing aid; during sintering, a portion of the carbon in the graphite diffused into the iron powder yielding a finished preform with a composition analogous to 1080 steel. These preforms were pressed and gravity sintered to obtain a relative density of approximately 0.60, as determined by simple mass and volume measurements. A second type of preform was fabricated from prealloyed 409 stainless steel powder (−80 mesh). The stainless steel preforms were pressed and sintered to yield a relative density of about 0.70.

The matrix used in this investigation was a modified 380 aluminium alloy, an age-hardenable Al–Si casting alloy. The composition of the 380 used in this investigation is given in Table I, the specific gravity is 2.65 $Mg\,m^{-3}$. No alloying elements were added to modify the silicon morphology.

2.2. Experimental methods

To infiltrate the porous sintered metal preforms with liquid 380 aluminium, a 200-ton Dake™ pressure casting press was used. The casting variables investigated were liquid metal temperature, maximum dwell pressure, and maximum infiltration velocity. During the casting operation, the punch reached maximum infiltration velocity before the dwell period was initiated. Thus, set by the infiltration velocity through Darcy's Law, the infiltrating pressure rose during infiltration to the maximum value assigned to the dwell period. The two metal casting temperatures (675 and 730 °C), maximum dwell pressures (88 and 164 MPa), and maximum infiltration velocities (0.21 and 1.69 $cm\,s^{-1}$) were systematically varied to evaluate their influence on composite properties.

From previous research [10–15], it was demonstrated that successful alloy infiltration requires that the reinforcing preforms exceed the liquidus temperature of the matrix alloy. For ceramic preforms, preheating the preforms in an air furnace prior to infiltration is possible. However, in the case of steel preforms, heating in a furnace would require the use of a protective atmosphere to avoid formation of an oxide film upon elevated temperature exposure. Such a film could inhibit subsequent liquid metal infiltration, which could possibly interfere with adhesion between the aluminium and reinforcements. Rather than using a furnace with a protective atmosphere, the sintered preforms were heated by immersing each preform in a bath of liquid 380 aluminium immediately prior to pressure casting. The duration of the immersion was also varied (30 and 45 s) to determine its effect on composite properties. The four variable processing parameters (liquid metal temperature, dwell pressure, infiltration velocity, and preform immersion time) were changed in random sequence through the use of a design-of-experiments scheme to avoid bias.

Following preheat dipping, the preform was rapidly transferred to the casting chamber and a predetermined amount of liquid 380 was forced under pressure into the casting chamber on top of the preform. The pressurization cycle was then initiated, and after being held under maximum pressure for 2 min in

TABLE I Composition of the modified 380 alloy

Si	Fe	Cu	Mn	Mg	Cr	Ni	Zn	Sn	Ti	Al
8.30	0.13	3.47	0.02	trace	trace	0.02	0.01	trace	0.01	88.00

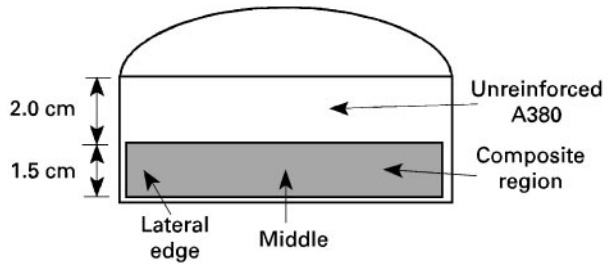

Figure 1 Schematic diagram of a cross-section through a cast composite.

a preheated die (275 °C), a cylindrical casting, approximately 10.6 cm in diameter by 3.5 cm tall, was produced. The infiltrated preform constituted the bottom 1.5 cm of the casting, with the remainder being unreinforced 380. A schematic diagram of a typical composite casting in cross-section is shown in Fig. 1.

After pressure casting, the reinforced castings were heat treated in air at 204 °C for 8 h (T5 temper). The castings were then sectioned parallel to the preform pressing direction and prepared for metallographic observation. The volume fractions of the reinforcement, matrix, and reaction phases were determined from these sections using a 11×11 grid in an optical microscope. The point counting measurements were performed in accordance to ASTM standard E562-89. Energy dispersive spectroscopy was also performed on selected slices to gain an understanding of the composition of the phases within the composite region.

To test the mechanical behaviour of the composites, room-temperature tensile tests were conducted. The tensile tests were performed following ASTM B557 using a MTS 880 computer-controlled TestStar™ test machine. The cylindrical tensile specimens were approximately 9 cm long and had a 2.54 cm gauge length having a 0.65 cm diameter. The specimens were gripped in hydraulic collet grips with great care taken to ensure proper alignment. The initial strain rate was $2 \times 10^{-3}\,s^{-1}$. Scanning electron microscopy (SEM) was performed on the fracture surfaces to gain an understanding of the failure mechanisms.

3. Results

3.1. Metallography

As a result of the considerable infiltration velocity coupled with the high fluidity of the silicon–aluminium alloy, significant preform infiltration was accomplished in each fabrication trial. The combination of a low maximum dwell pressure (88 MPa) and a low maximum infiltration velocity ($0.21\,cm\,s^{-1}$) did not produce complete infiltration in every case; the bottom corners of the preform remained void of aluminium alloy for these processing conditions. This result could have been caused by excessive freezing of the 380 alloy before complete infiltration occurred. All other combinations of parameters yielded complete infiltration. Also, no evidence of preform cracking or deformation was observed.

Optical micrographs of sectioned composites are shown in Figs 2 and 3. The composite regions examined metallographically are indicated on the schematic diagram in Fig. 1: middle and lateral edge. Fig. 2a and b show the typical microstructure at the middle and lateral edge, respectively, of the steel-reinforced composite. Fig. 3a and b display the same areas for the stainless steel-reinforced composite. Both composites were fabricated using the same casting conditions: melt temperature of 730 °C, dip duration of 30 s, maximum dwell pressure of 88 MPa, and maximum infiltration velocity of $1.69\,cm\,s^{-1}$.

The micrographs in Fig. 2 show a reaction phase surrounding the steel powder particles. Previous work [6, 8, 9, 16] on steel-reinforced aluminium MMCs has shown this phase to be an intermetallic phase containing aluminium and iron. This reaction phase was more abundant in the middle region of the composite (Fig. 2a) which cooled at the slowest rate and, as a result, was exposed to liquid aluminium for the longest time. Near the periphery (Fig. 2b) and near the bottom of the composite, where the casting was in contact with the die wall, less reaction phase was found in all cases.

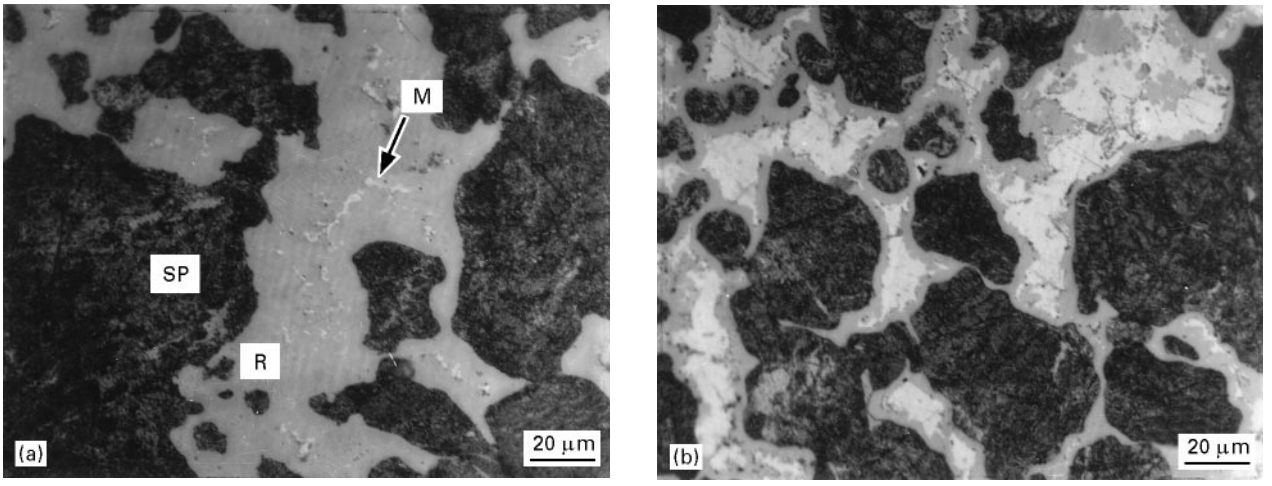

Figure 2 Optical photomicrographs of steel-reinforced composites. SP, the steel preform; R, reaction phase; M, the aluminium matrix (a) The middle of the composite region, (b) the lateral edge.

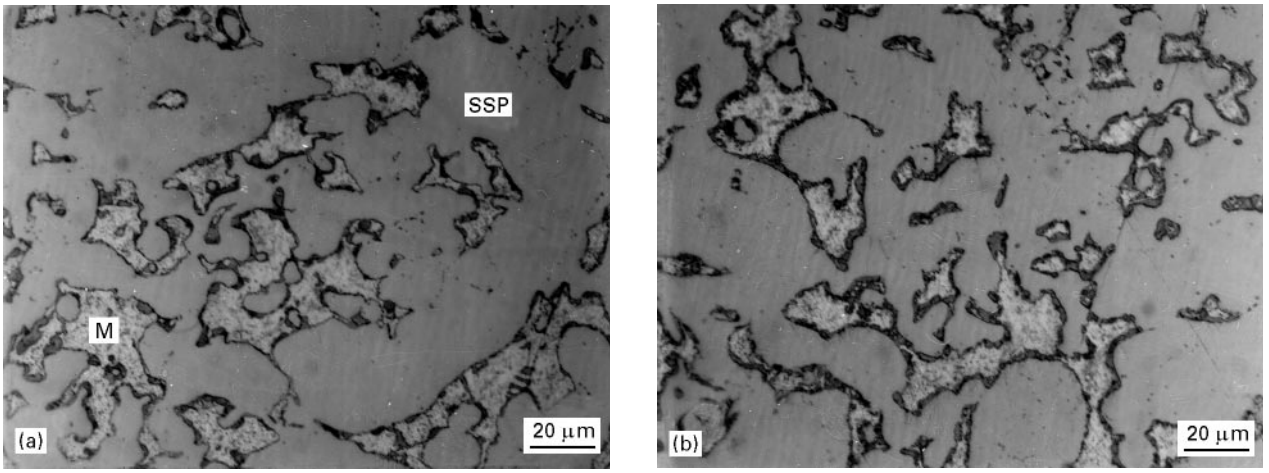

Figure 3 Optical photomicrographs of stainless steel-reinforced composites. SSP, the stainless steel preform; M, the aluminium matrix. The dark phase outlining the preform particles is the reaction phase. (a) The middle of the composite region, (b) the lateral edge.

With the stainless steel reinforcements, however, the extent of intermetallic phase formed between the preform particles and aluminium matrix was greatly diminished (Fig. 3). Unlike the steel-reinforced composites, no noticeable difference in the amount of intermetallic can be discerned between the middle (Fig. 3a) and peripheral (Fig. 3b) regions of the composite.

3.2. Energy dispersive spectroscopy

Figs 4 and 5 display the results from the composition analysis of the steel- and stainless steel-reinforced composites, respectively. Both scans have been divided into three distinct regions: preform particle, reaction phase, and 380 aluminium matrix. Back-scattered electron micrographs of the two areas examined are included, with the locations of the composition traces indicated. The composition analyses were performed using the same cross-sections prepared for optical metallography.

The composition scan across the reinforcement/matrix interface in the steel-reinforced composite (Fig. 4) indicates that a compound containing significant amounts of iron and aluminium, and a small amount of silicon, formed during fabrication. The

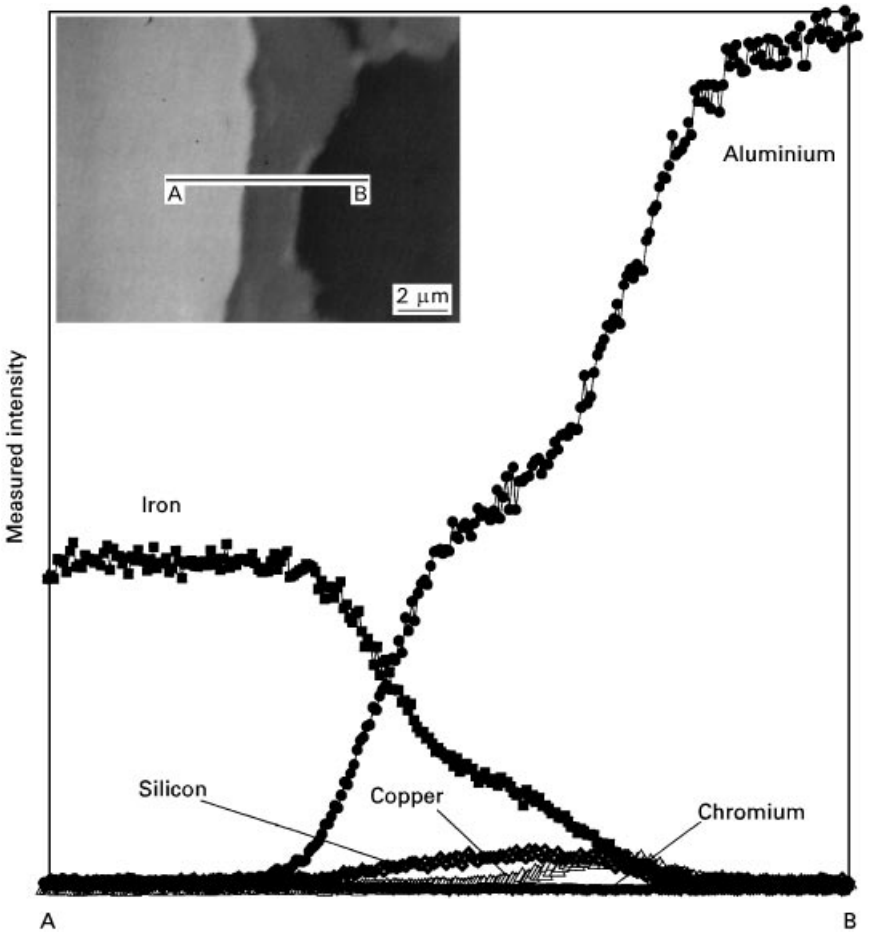

Figure 4 Composition scan across the reinforcement/matrix interface in a steel-reinforced cast composite with backscattered electron image of scanned area (inset). The composition scan is indicated on the micrograph (A–B). △ copper; ◇ silicon; ▼chromium; ■ iron and ● aluminium

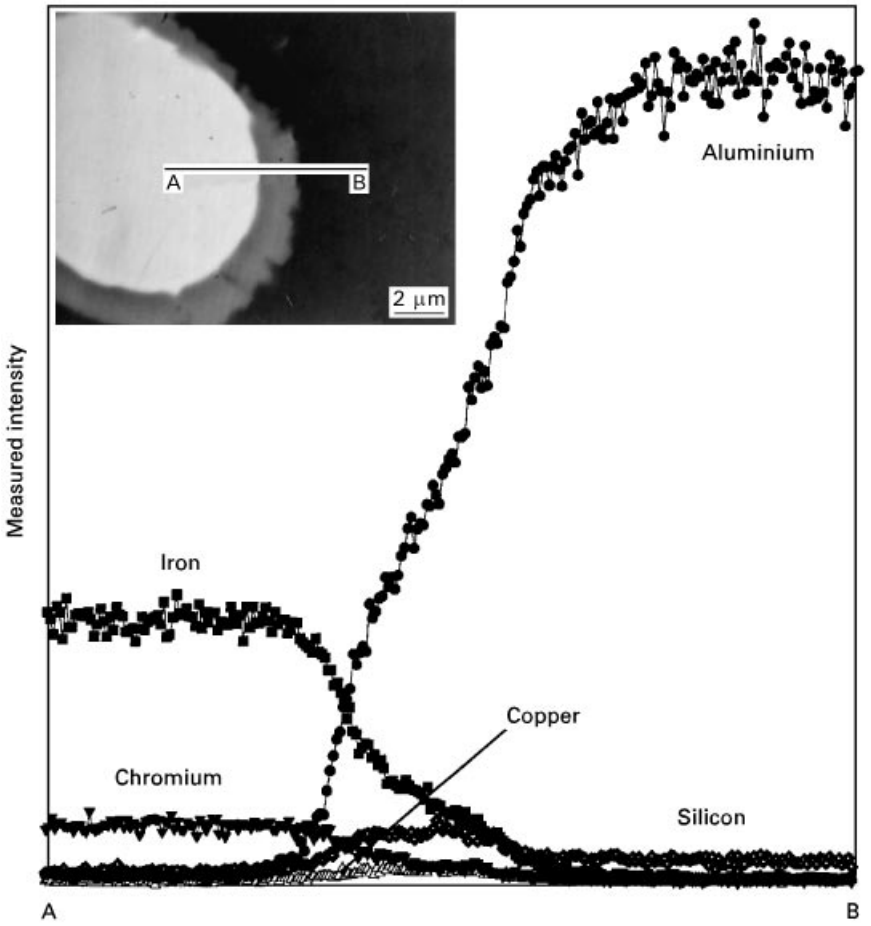

Figure 5 Composition scan across the reinforcement/matrix interface in a stainless steel-reinforced cast composite with backscattered electron image of scanned area (inset). The composition scan is indicated on the micrograph (A–B). △ copper; ◇ silicon; ▼chromium; ■ iron and ● aluminium.

quantitative composition of the reaction phase was not evaluated. However, the measurements indicate that the atomic fraction of iron present in the reaction phase declines from the steel preform particle to the matrix phase. In the reaction phase, the iron content appears to consist of two distinct sections of differing slope.

In contrast, the aluminium trace indicates an increase in the amount of aluminium as the scan passes from the preform particle to the matrix. A similar, bilinear behaviour is observed with the aluminium trace in the reaction phase. Furthermore, the amount of silicon appears to reach a maximum within the reaction phase.

On either side of the reaction phase, the composition measurements detected the expected constituent elements for the steel reinforcements (iron) and 380 alloy (aluminium, silicon, and copper). As expected, no chromium was detected.

Fig. 5 shows a similar composition analysis performed using the stainless steel-reinforced composite. Again, although a qualitative evaluation of the reaction phase was not performed, the phase contains significant amounts of iron and aluminium with a small amount of silicon. The reaction phase also appears to contain very little chromium, with the fraction steadily decreasing from the stainless steel preform to the matrix phase.

Similar to the previous composition analysis, the fraction of iron decreases from the preform particle to the aluminium matrix and, conversely, the fraction of aluminium increases. Again, the composition trace indicates two distinct regions within the reaction phase where the iron and aluminium traces have different slopes. Also, the maximum amount of silicon detected appears to lie within the reaction phase. The elements characteristic of the stainless steel reinforcement (iron and chromium) and aluminium 380 alloy (aluminium, silicon, and copper) were detected on either side of the reaction phase.

From the backscattered images and composition analyses, the thickness or volume fraction of the reaction phase appears to be approximately the same for the steel- and stainless steel-reinforced composites. However, the measurements were not taken at the same regions within the composite section. Therefore, a general comparison of the extent of reaction cannot be made between the steel- and stainless steel-reinforced composites using composition measurements.

3.3. Tensile tests

Tensile test results are listed in Tables II–V. Tables II and III contain the test results for the steel-reinforced composites fabricated at different melt temperatures; Tables IV and V provide the same information for the stainless steel-reinforced composites. The values listed in the tables are the average of results obtained from two tensile tests performed for each condition. Also included in the tables is the volume fraction of

TABLE II Steel-reinforced aluminium MMC, 730 °C casting temperature

Dip time (s)	Max. dwell pressure (MPa)	Max. infiltration velocity ($cm\ min^{-1}$)	Yield strength (MPa)	Tensile strength (MPa)	Elastic modulus (GPa)	Elongation (%)	Volume fraction of reaction phase (%)
30	88	12.7	–	191.19	–	0.035	35.08
	88	101.6	–	198.94	197.12	0.035	37.70
	164	12.7	–	218.63	178.85	0.100	32.77
	164	101.6	–	230.41	193.74	0.070	37.57
45	88	12.7	–	194.09	193.95	0.070	39.92
	88	101.6	–	214.29	186.64	0.050	36.64
	164	12.7	–	207.35	204.91	0.065	39.76
	164	101.6	–	211.07	203.47	0.085	35.03

TABLE III Steel-reinforced aluminium MMC, 675 °C casting temperature

Dip time (s)	Max. dwell pressure (MPa)	Max. infiltration velocity ($cm\ min^{-1}$)	Yield strength (MPa)	Tensile strength (MPa)	Elastic modulus (GPa)	Elongation (%)	Volume fraction of reaction phase (%)
30	88	12.7	–	198.94	170.92	0.060	19.59
	88	101.6	–	191.24	172.16	0.060	29.47
	164	12.7	–	267.45	159.34	0.085	17.85
	164	101.6	–	305.90	170.72	0.140	17.69
45	88	12.7	–	182.69	181.75	0.040	32.27
	88	101.6	–	294.67	159.82	0.095	14.53
	164	12.7	–	236.17	183.47	0.030	30.29
	164	101.6	–	202.69	199.40	0.095	31.51

TABLE IV Stainless steel-reinforced aluminium MMC, 730 °C casting temperature

Dip time (s)	Max. dwell pressure (MPa)	Max. infiltration velocity ($cm\ min^{-1}$)	Yield strength (MPa)	Tensile strength (MPa)	Elastic modulus (GPa)	Elongation (%)	Volume fraction of reaction phase (%)
30	88	12.7	260.46	390.31	169.47	3.28	13.26
	88	101.6	244.51	357.91	157.13	2.01	12.81
	164	12.7	302.03	371.48	183.95	2.00	16.53
	164	101.6	289.49	382.43	174.92	2.32	21.86
45	88	12.7	243.95	384.83	177.68	3.48	18.43
	88	101.6	294.48	336.97	184.99	1.83	21.15
	164	12.7	279.11	378.82	174.65	2.36	12.98
	164	101.6	328.90	353.68	178.78	0.770	22.05

TABLE V Stainless steel-reinforced aluminium MMC, 675 °C casting temperature

Dip time (s)	Max. dwell pressure (MPa)	Max. infiltration velocity ($cm\ min^{-1}$)	Yield strength (MPa)	Tensile strength (MPa)	Elastic modulus (GPa)	Elongation (%)	Volume fraction of reaction phase (%)
30	88	12.7	229.27	398.52	164.03	6.84	4.54
	88	101.6	229.36	393.90	160.75	5.11	4.75
	164	12.7	251.15	393.98	158.30	5.13	3.93
	164	101.6	298.28	409.41	165.54	3.32	4.42
45	88	12.7	230.13	405.48	162.92	6.81	4.96
	88	101.6	244.83	379.74	169.06	3.14	5.99
	164	12.7	248.49	406.17	166.72	6.02	7.27
	164	101.6	248.54	400.66	167.89	5.16	9.75

reaction phase measured from the point-counting analysis.

Tensile tests were also performed on the unreinforced 380 alloy, produced by pressure casting and subjected to a T5 tempering treatment. The unreinforced castings were produced using two different casting conditions. One set of castings was made with a dwell pressure of 164 MPa and a punch velocity of

1.60 cm s^{-1} and the other set was fabricated with a dwell pressure of 88 MPa and a punch velocity of 0.21 cm s^{-1}. However, unlike their reinforced counterparts, the tensile properties of the unreinforced 380 castings were unaffected by the casting conditions. The average properties measured for 380 are listed in Table VI. Although the yield strength obtained is lower, both the tensile strength and elongation values obtained in the present study are greater than those available in the literature for squeeze cast 380 aluminium. For example, Lynch *et al.* [19] obtained a yield strength of 188 MPa, a tensile strength of 240 MPa, and an elongation of 2.1%. It is possible that the results given in the literature were obtained from smaller castings, in which case the cooling rate would be expected to cause a difference in the tensile properties. To assist comparison of the composite properties to the constituent phase properties. Table VI also lists the tensile properties of 1080 steel and 409 stainless steel in the fully dense and annealed state.

The effect of casting conditions on the mechanical properties can be observed in Tables II–V. Although there is a considerable difference in the two maximum infiltration velocities, maximum dwell pressures, and dip durations, there is no significant difference in the resulting mechanical properties. For those three variables, no definitive trend can be identified indicating which condition produces a superior composite. In contrast, melt temperature has a significant reproducible effect on mechanical properties: a lower melt temperature (675 °C) appears to produce superior tensile strength and elongation. The largest effect of casting temperature on composite properties can be observed in the results with stainless steel reinforcements (Tables IV and V).

The steel-reinforced composites (Tables II and III) exhibited very brittle behaviour. Because the steel-reinforced composite materials did not achieve 0.2% plastic strain, a 0.2% offset yield strength cannot be reported for these composites. Thus, in Tables II and III, no offset yield strength values are indicated for the steel-reinforced composites. The mechanical properties exhibited by the steel-reinforced composites are also considerably poorer than the properties of the annealed 1080 steel listed in Table VI. In fact, the tensile strengths of the composite specimens were not that much greater than the tensile strength of the unreinforced 380 alloy. This result indicates that the steel reinforcement does not contribute appreciably to the tensile strength of the composite. However, compared to the unreinforced 380 alloy, the steel-reinforced composites had notably higher Young's moduli.

The stainless steel-reinforced composites (Tables IV and V) displayed enhanced tensile strength and elongation values compared to their steel-reinforced counterparts, while exhibiting slightly lower moduli. The stainless steel-reinforced composites had slightly lower moduli and significantly lower elongation values than fully dense annealed 409 stainless steel, but comparable yield and tensile strengths. Thus, in contrast to the steel powder particles, the stainless steel powder particles impart substantial strength to the aluminium matrix, especially for the lower melt temperature of 675 °C.

Compared to the tensile strength of the unreinforced 380, the tensile strength of the stainless steel-reinforced composites was significantly higher. Also, for the lower melt temperature, the elongation and tensile strength of the composites exceeded those of the unreinforced 380 alloy. This suggests that a bond exists between the matrix and stainless steel reinforcing phase, and the ductile stainless steel reinforcing phase contributes significantly to the composite properties.

3.4. Scanning electron microscopy of fracture surfaces

To gain an understanding of the fracture mechanism(s), tensile specimens were examined in an SEM after testing. Fig. 6 shows scanning electron micrographs of a steel-reinforced composite fracture surface of a tensile specimen. Fig. 6a and b show the fracture surface and the underlying microstructure of the composite specimen. Fig. 6c shows the microstructure of the same sample further away from the fracture surface.

The micrographs in Fig. 6a and b show that failure in the steel-reinforced composite occurred adjacent to the powder particle/matrix interface, within the reaction phase. In addition to the crack that caused failure of the specimen, extensive cracking was observed beneath the fracture surface. In these cases, cracks propagated along the particle/matrix interface within the reaction phase (Fig. 6b). Combining these observations with the tensile test results suggests that the brittle intermetallic phase preferentially cracks prior to significant plastic flow of the matrix or reinforcement phase.

Away from the fracture surface, subcritical cracks are observed within the intermetallic phase, as displayed in Fig. 6c. This crack may have initiated at the pore between the reinforcing powder particles. After propagating some distance within the reaction phase, the crack propagates between the matrix and the reaction phase, in contrast to propagating solely within the reaction phase as observed in Fig. 6b.

Fig. 7 displays the fracture surface of a stainless steel-reinforced composite. The micrograph in Fig. 7a shows the fracture surface and adjacent polished microstructure. Fig. 7b shows a portion of the polished tensile specimen microstructure away from the fracture surface.

As with the steel-reinforced composites, failure developed within the interfacial intermetallic phase in the stainless steel-reinforced composites (Fig. 7a). In previous studies [5, 6] of stainless steel-reinforced aluminium composites, it was observed that the failure did not occur at the fibre/matrix interface; rather, failure occurred in the stainless steel wires themselves. This discrepancy in failure mode can be explained through the geometry of the reinforcement phases. When wires, or long fibres, are used, load transfer from the matrix to the reinforcement occurs and the stress in the reinforcing phase may substantially

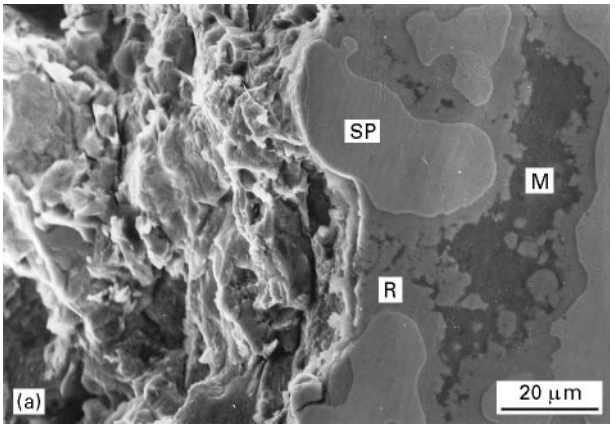

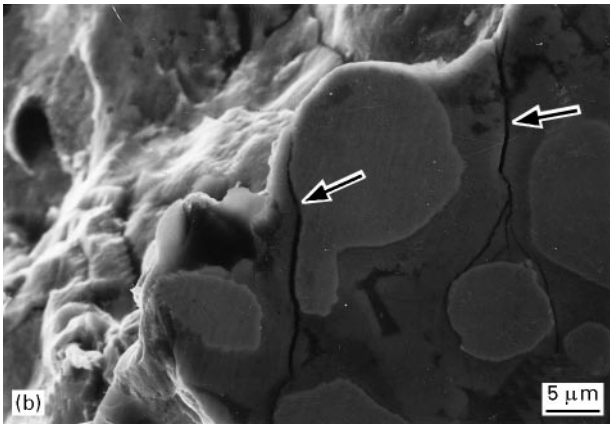

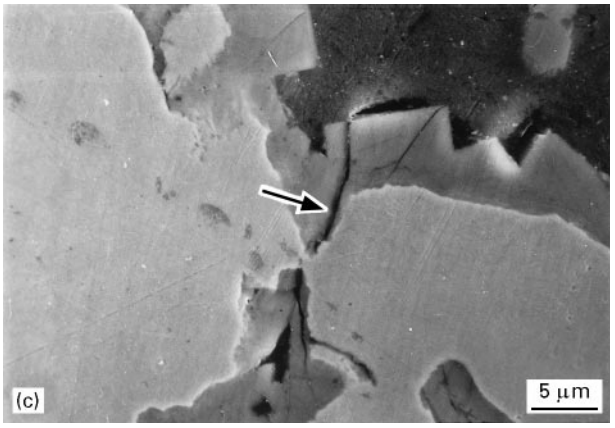

Figure 6 Scanning electron micrographs of fractured tensile specimen in steel-reinforced composite. SP, the steel preform; R, the reaction phase; M, the aluminium matrix. (a) The microstructure (right-hand side) adjacent to the fracture surface (left-hand side), (b) cracks (indicated by arrows) adjacent to the fracture surface; (c) a crack (indicated by arrow) away from the fracture surface.

exceed the average stress. Ideally, failure finally occurs when the composite strain reaches the ultimate tensile strain of the fibre reinforcements. However, in the present case, the reinforcing phase is in particulate form which limits load transfer between the reinforcements and matrix.

As in the steel-reinforced composites, cracks can be seen away from the fracture surface along the particle/matrix interface (Fig. 7b). However, because the volume fraction of reaction phase is less in the stainless steel-reinforced composites, the cracks only propagate a short distance and do not link up with neighbouring cracks.

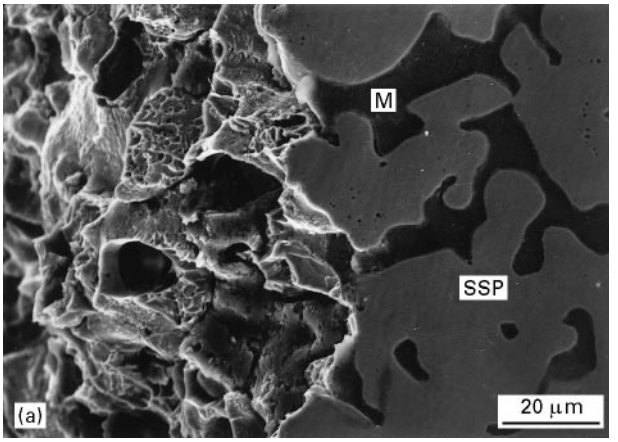

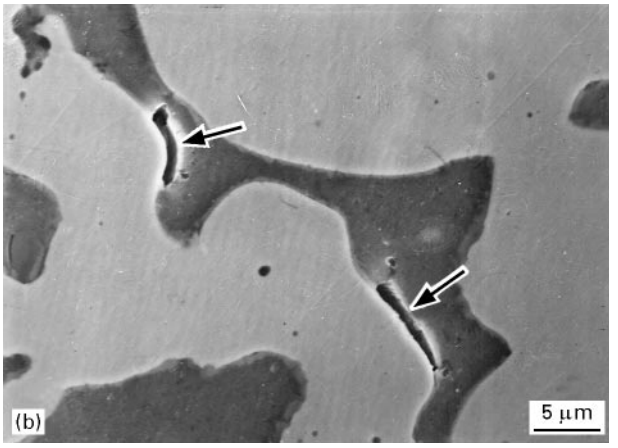

Figure 7 Scanning electron micrographs of a fractured tensile specimen in stainless steel-reinforced composite. SSP, the stainless steel preform; M, the aluminium matrix. (a) The microstructure (right-hand side) adjacent to the fracture surface (left-hand side), (b) cracks (indicated by arrows) away from the fracture surface.

4. Discussion

4.1. Effect of casting conditions on microstructure

As indicated in Table I, the aluminium matrix contains significant amounts of silicon (8.3%) and copper (3.5%). Silicon has been shown [20] to restrict greatly the growth of the reaction phase that forms when steel is exposed to liquid aluminium. The presence of silicon has also caused the formation of iron–silicon phases within the reaction phase. Copper is also reported to restrict the growth of the reaction phase, though not as dramatically as silicon [20].

The micrographs in Fig. 2 indicate that a considerable reduction in the volume fraction of reaction phase is observed at the periphery of the steel-reinforced composite. These composite regions were subjected to a higher cooling rate due to their proximity to the die wall. Also, a noticeable reduction in the amount of intermetallic phase was detected in the composites fabricated at the lower metal temperature (675 °C). These observations indicate that extended exposure of the steel reinforcement to liquid aluminium is necessary for substantial growth of the reaction phase. This behaviour is consistent with previous research involving cast aluminium alloy composites containing ferrous reinforcements [5, 6, 9].

In contrast, from the micrographs in Fig. 3, the volume fraction of reaction phase does not differ significantly between the middle region and lateral edges in the stainless steel composites. This observation indicates that a different mechanism than rapid cooling near the die wall inhibits formation of reaction phase in the stainless steel-reinforced MMCs. Similar to the steel-reinforced composites, a lower volume fraction of intermetallic was found throughout in the stainless steel-reinforced composites when the lower casting temperature was used.

In previous research [21], it was shown that a dense, adherent oxide present on the reinforcing phase could provide a diffusion barrier between the reinforcement and infiltrating molten aluminium, thereby inhibiting formation of a reaction phase. The major alloying element in stainless steels, chromium, forms a stable, adhesive oxide on the surface which could act as such a barrier. In contrast, iron oxide does not exhibit the same thermodynamic stability as the chromium oxide, and, therefore, does not act as an effective barrier between the aluminium and powder particles in the case of the steel reinforcements [21]. The reaction inhibiting effect of chromium in the iron-based reinforcements is similar to the retardation of intermetallic phase growth in steels containing chromium during aluminizing [20].

The greater volume fraction of reinforcement in the stainless steel-reinforced composites also may have influenced the amount of intermetallic present. When a larger volume fraction of reinforcement is present, more material is available to extract heat from the liquid aluminium alloy, thereby decreasing the amount of time that the molten alloy remains in contact with the preform. This effect may also inhibit intermetallic growth [9].

Whereas the melt temperature appears to affect the volume fraction of reaction phase present, the other variable casting parameters did not appear to have a dramatic effect on the composite microstructure, within the ranges evaluated in the present study. No significant variation in the volume fraction of reaction phase was observed as the dip duration, maximum dwell pressure, and maximum infiltration velocity were systematically changed.

Although the volume fraction of the reaction phase is not the same in the steel- and stainless steel-reinforced composites, the composition of the reaction phase appears to be very similar. From the composition traces given in Figs 4 and 5, the reaction phase contains significant amounts of iron and aluminium, with a smaller amount of silicon. The reaction phase in the stainless steel composites may also contain some chromium, but the concentration quickly decreases from the powder particle to the aluminium matrix.

In both composite types, the iron and aluminium traces appear to be divided into two regions of different slope. This change in the slope of the iron and aluminium scans could indicate that two separate intermetallic compounds constitute the reaction phase. Previous work [6, 8] has shown that this reaction phase is comprised of a number of iron–aluminium intermetallics, though the compositions were not quantitatively evaluated.

4.2. Effect of microstructure on properties

Because the preforms are comprised of different materials and relative densities, the strength of the uninfiltrated preforms must be known to compare accurately the resulting composite properties. Two simple expressions for the strength, S, of a porous body as a function of relative density, D, are

$$S = S_0 D^m \tag{1}$$

$$S = S_0 e^{-b(1-D)} \tag{2}$$

where S_0 is the strength of the fully dense material and m and b are empirical constants [22]. For iron-based metals, m is reported to be approximately 6 and b is about 5 [22]; these values will be used in the current application. Using the tensile strength values given in Table VI as S_0, both equations will be used to estimate the tensile strength of the 1080 steel and the 409 stainless steel preforms.

From Equation 1 and at a relative density of 0.6, the tensile strength of the porous 1080 steel preforms is predicted to be approximately 29 MPa. Equation 2, however, yields a slighter higher tensile strength estimate of 83 MPa for the steel preforms. For the stainless steel preforms at a relative density of 0.7, Equation 1 generates a tensile strength of 45 MPa, while Equation 2 produces a value of 85 MPa. Thus, although the fully dense, wrought materials have significantly different tensile strengths, the different relative densities of the powder metallurgy reinforcements produce similar preform strength estimates. However, as seen in Tables II–V, the stainless steel-reinforced composites have considerably greater strength values compared to their steel-reinforced counterparts.

The superior tensile properties demonstrated by the stainless steel-reinforced composites correlates with the volume fraction of reaction phase present, as shown in the last column in Tables II–V. The composites with steel reinforcements contained a considerable volume fraction of reaction phase, with an overall average of approximately 30%. A significantly greater amount formed in the steel-reinforced composites at the higher casting temperature (730 °C), when the average volume fraction increased to 37%. The presence of the reaction phase around the powder particles suggests that an adequate bond exists between the reinforcing phase and matrix alloy. With a sufficient bond, the strength of the composite should be greater than the strength of the unreinforced matrix phase.

TABLE VI Mechanical properties of fully dense materials

Material	Yield strength (MPa)	Tensile strength (MPa)	Modulus (GPa)	Elongation (%)
380	121	248	66.9	4.0
1080 [17]	376	615	210	25
409 ss [18]	205	380	197	20

However, present in such large amounts, this intermetallic phase renders the reinforcement/matrix interface brittle, limiting the beneficial effect of the stronger reinforcing phase [6]. In effect, the reaction phase fails before significant strength enhancement occurs. Thus, although the formation of this intermetallic phase may enhance bonding between the two phases, it fails prematurely, thereby causing the composite to exhibit extremely low elongation values.

Conversely, in the stainless steel-reinforced composites, the volume fraction of reaction phase is relatively low, especially at the lower casting temperature (675 °C). Although the yield strength seems to be enhanced by the increased volume fraction of reaction phase, both the elongation and ultimate tensile strength values appear to be inversely proportional to volume fraction of reaction phase. Unlike the steel-reinforced composites, the stainless steel reinforcements do not contain a high volume fraction of reaction phase and premature fracture does not limit the ability to observe a reinforcing effect.

The degradation of the composite properties caused by the reaction phase is supported by the scanning electron micrographs in Figs 6 and 7. The micrographs exhibit failure occurring exclusively within the reaction phase. In the case of the steel-reinforced composites, the high volume fraction of reaction phase allows the crack to propagate readily, link up with other cracks, and cause premature failure. In effect, fracture of the specimen occurs before the strength of the reinforcement can be realized in the steel-reinforced composites.

Cracks also form within the reaction phase in the stainless steel-reinforced composites. However, compared to the steel-reinforced composites, the volume fraction of the reaction phase in the stainless steel composites is considerably lower, and the cracking appears (in the plane of polish) to be localized. As a result, strength enhancement from the reinforcing stainless steel powder particles occurs before development of critical-length cracks.

The adverse effect that the high volume fraction of intermetallic has on the ductility of the stainless steel-reinforced composites is illustrated in Fig. 8. The graph also displays the extremely low elongation values exhibited by the steel-reinforced composites. Clearly, minimizing the volume fraction of reaction phase is beneficial for ductility. These results are consistent with previous investigations of the growth of intermetallic layers on stainless steel reinforcements in an aluminium matrix [6, 8, 16].

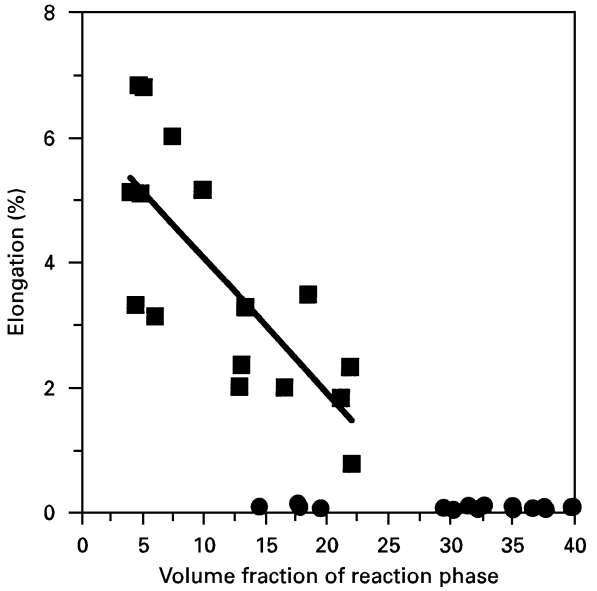

Figure 8 Percentage elongation plotted against volume fraction of reaction phase for both the (■) stainless steel-reinforced composites and (●) steel-reinforced composites.

5. Conclusions

In the current investigation, an aluminium casting alloy was successfully reinforced with sintered metal preforms through the squeeze casting technique. Two types of preforms were used: 0.8% C steel (relative density of 0.6) and stainless steel (relative density of 0.7). Fabricated under a number of casting conditions, the composites exhibited varying microstructures and mechanical properties. From the experiments performed and observations made, several conclusions can be formulated.

1. During the high-temperature processing of the aluminium MMCs, a reaction phase containing iron, aluminium, and silicon formed around the preform particles, with an increased volume fraction observed in the steel-reinforced composites.
2. For both reinforcement types, melt temperature appeared to have a strong effect on composite properties, with the lower casting temperatures producing superior composites.
3. From the tensile tests performed on the aluminium matrix composites, the stainless steel reinforcement provides improved mechanical properties compared to a 0.8% C steel reinforcement. The superior properties of the stainless steel-reinforced composites can be correlated to the volume fraction of reaction phase that formed around the powder particles during processing.

Acknowledgements

The authors thank the General Motors Corporation for providing the funding and materials for this research. The powder preforms were fabricated by Powder-Tech Associates, Inc., North Andover, MA. The tensile tests were performed by Ed Huested at the General Motors Powertrain Group Casting Technology Center, Saginaw, MI. The authors also thank Professor R. German for helpful discussions concerning the powder metallurgy preforms, and Doctor C. Coleman Jones for his numerous contributions.

References

1. F. M. HOSKING, F. FOLGAR PORTILLO, R. WUNDERLIN and R. MEHRABIAN, *J. Mater. Sci.* **17** (1982) 477.
2. M. S. HU, J. YANG, H. C. CAO, A. G. EVANS and R. MEHRABIAN, *Acta. Metall. Mater.* **40** (1992) 2315.

3. M. J. O'CONNER, F. E. WAWNER and C. C. JONES, *J. Mater. Sci.* **31** (1996) 164.
4. T. W. CLYNE, M. G. BADER, G. R. CAPPLEMAN and P. A. HUBERT, *ibid.* **20** (1985) 85.
5. D. CRATCHLEY, *Powder Metall.* **11** (1963) 59.
6. R. B. BHAGAT, *Metall. Trans.* **16A** (1985) 623.
7. *Idem*, *AIAA J.* **23** (1984) 912.
8. *Idem*, *Composites* **19** (1988) 393.
9. C. COLIN, Y. MARCHAL, F. BOLAND and F. DELANNAY, *J. Phys. IV* **3** (1993) 1749.
10. A. MORTENSEN, L. J. MASUR, J. A. CORNIE and M. C. FLEMINGS, *Metall. Trans.* **20A** (1989) 2535.
11. L. J. MASUR, A. MORTENSEN, J. A. CORNIE and M. C. FLEMINGS, *ibid.* **20A** (1989) 2549.
12. A. MORTENSEN and V. MICHAUD, *ibid.* **21A** (1990) 2059.
13. V. J. MICHAUD and A. MORTENSEN, *ibid.* **23A** (1992) 2263.
14. P. JARRY, V. J. MICHAUD, A. MORTENSEN, A. DUBUS and R. TIRARD-COLLET, *ibid*, **23A** (1992) 2281.
15. T. W. CLYNE and J. F. MASON, *ibid.* **18A** (1987) 1519.
16. R. B. BHAGAT, *J. Mater. Sci.* **24** (1989) 1496.
17. C. MITCHELL, in "Metals Handbook, Desk Edition" edited by H. Boyer and T. Gall (ASM International, OH, 1985) p. 420.
18. J. R. DAVIS, in "Stainless Steels" edited by J. R. Davis and Davis and Associates (ASM International, OH. 1994) p. 21.
19. R. F. LYNCH, R. P. OLLEY and P. C. J. GALLAGHER, *Trans. AFS* **83** (1975) 569.
20. V. R. RYABOV, in "Aluminizing of Steel" edited by V. S. Kothekar (Oxonian Press, New Delhi, 1985).
21. F. DELANNAY, L. FROYEN and A. DERUYTTERE, in "Cast Reinforced Metal Composites" edited by S. G. Fishman and A. K. Dhingra (ASM International, 1988) p. 83.
22. F. P. KNUDSEN, *J. Am. Ceram. Soc.* **42** (1959) 376.

Received 20 February
and accepted 29 May 1997